Supplementary Figures and Tables

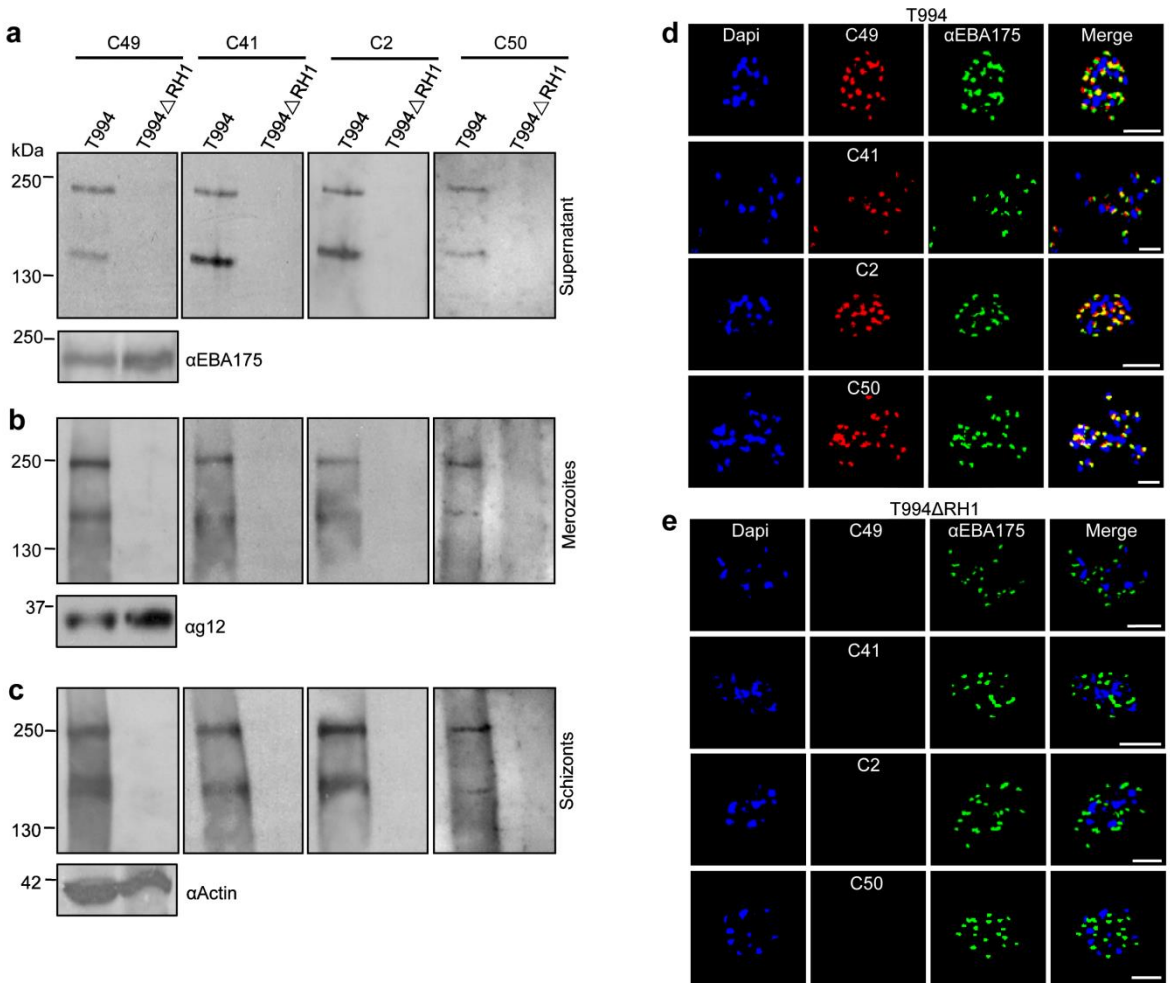

Supplementary Figure S1: PfRH1 mAbs specifically recognize native PfRH1. (**a**)-(**c**) PfRH1 mAbs specifically recognize full length PfRH1. Western blot analysis of T994 and T994ΔRH1 culture supernatants (**a**) merozoites extracts (**b**) and schizonts extracts (**c**) probed with PfRH1 mAbs. The expected protein of about 240 kDa and its processing product 140 kDa were detected by mAbs C49, C41, C2 and C50 in T994 only. Loading controls such as rabbit α-EBA175, mouse mAb g12and rabbit α-Actin, are presented at the bottom of (**a**)-(**c**) respectively. Molecular sizes are indicated on the left (in kDa). Double-staining IFAs of T994 (**d**) and T994ΔRH1(**e**). Smear of late stage schizonts were incubated with C49, C41, C2 or C50 (second column, red) and rabbit α-EBA175 (third column, green). Parasite nuclei were stained with DAPI (blue). In the merged images, areas of overlap between the red and the green signals are shown in yellow. Scale bars = 5 μM.

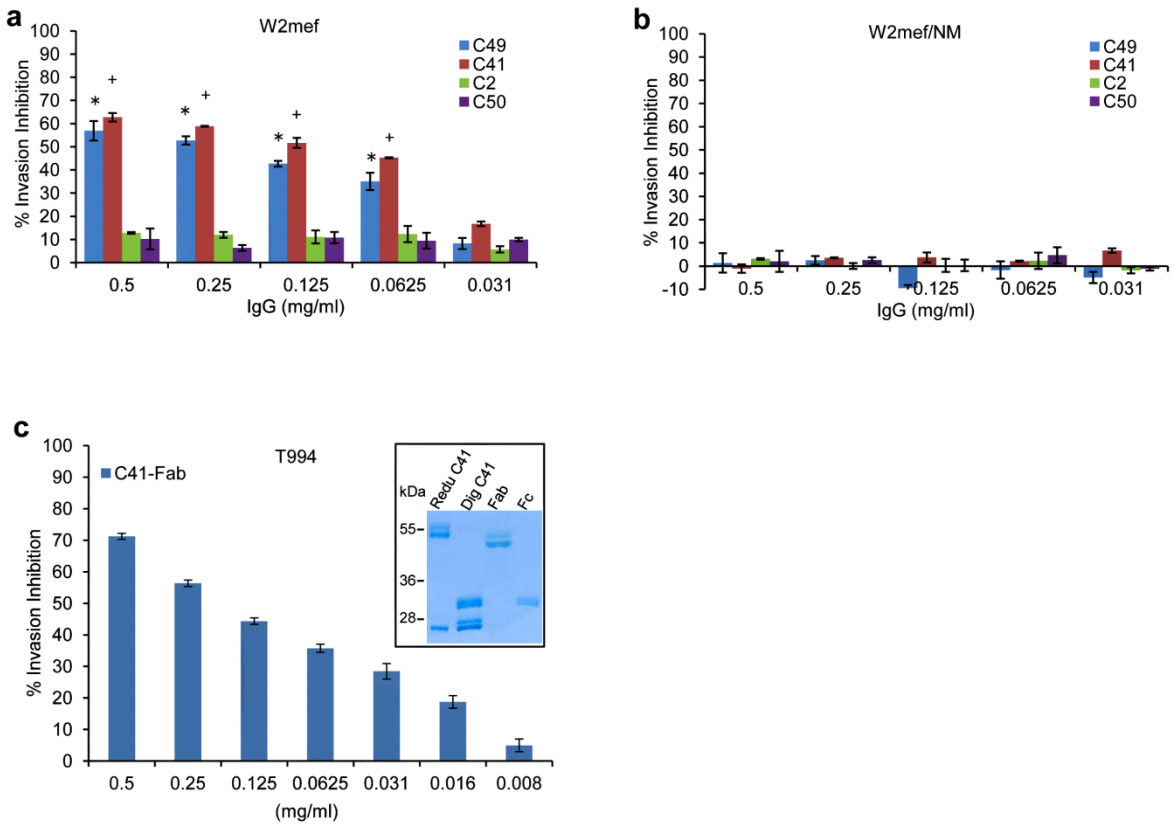

Supplementary Figure S2: Invasion inhibition assay. Bar charts represent the invasion inhibition in the presence of PfRH1 mAbsC49, C41, C2 and C50 in W2mef (**a**) and W2mef/NM (**b**) respectively. * or $^{+}$ $P \leq 0.0009$ by one-way ANOVA, indicating the significant different between the PfRH1 inhibitory mAbs (C49 or C41) and non-inhibitory mAbs (C2 and C50). (**c**) mAbs C41 Fab fragment significantly block invasion in T994 parasite in a dose-dependent manner. Purified C41 Fab fragment was analyzed by SDS-PAGE and stained with coomassie blue (shown in insert of (**c**)). C41 Fab (Fab) fragment was prepared under nonreducing conditions whereas C41 IgG (Redu C41), digested C41 IgG (Dig C41) and C41 Fc fragment (Fc) were prepared under reducing conditions. Reduced C41 IgG results in two bands of ~55and 25kDa. The Fab typically migrates around 50kDa. The presence of Fc at 28-30kDa confirms digestion of IgG. Molecular sizes are indicated on the left (in kDa). All mAbs as well as C41 Fab were used at final concentration from 0.5 down to 0.031 mg/ml. Bar charts show mean ±s.e.m.; $n = 3$.

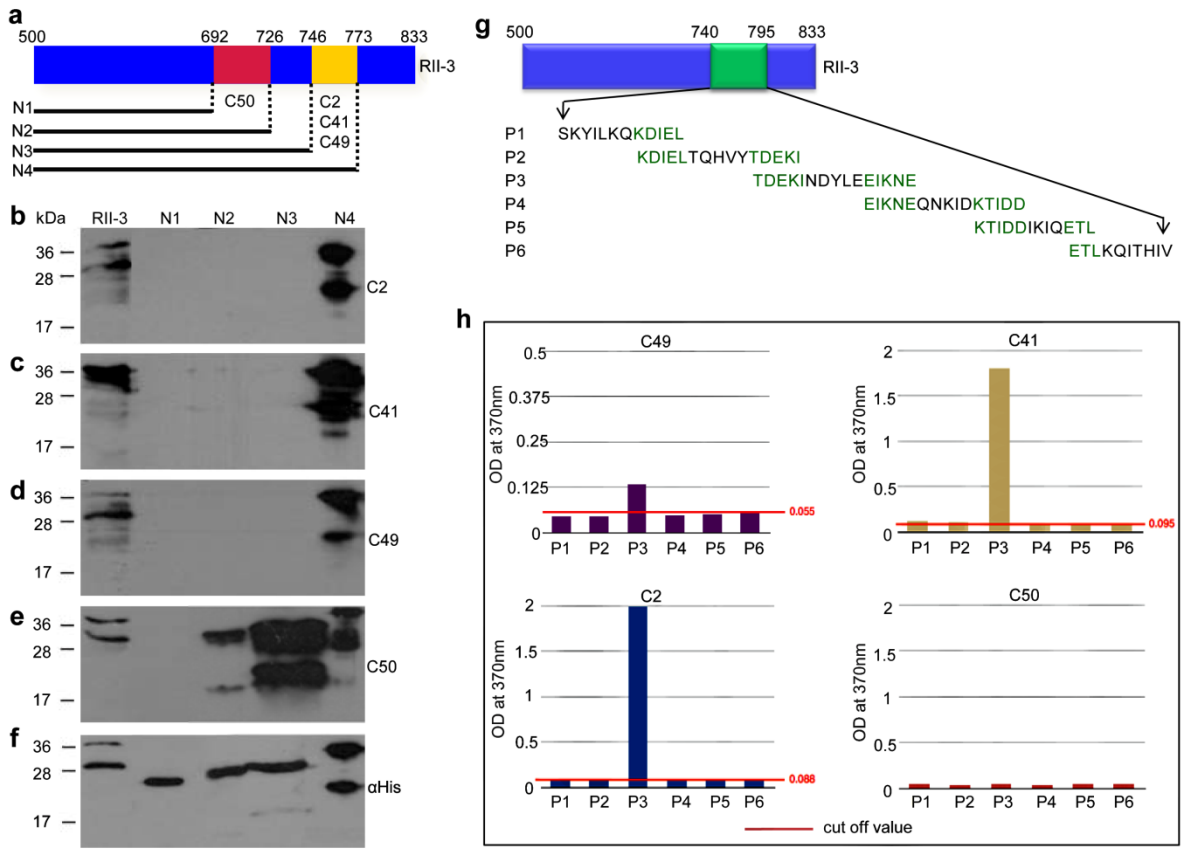

Supplementary Figure S3: Epitope mapping of erythrocyte binding region RII-3 using biotinylated peptides. (**a**) Chimeric N-terminal overlap fragments derived from RII-3 encompassing amino acids 500 to 833 (blue), named N1, N2, N3 and N4 (black line). N1 to N4 start from 500aa and end at: 692aa for N1, 726aa for N2, 746aa for N3 and 773 for N4. (**b-f**) Screening of mAbs C2 (**b**), C41 (**c**), C49 (**d**) and C50 (**e**) to different recombinant proteins including RII-3 and N1 to N4 respectively by Western blot analysis. Anti His-tag mAbs (αHis) was used as loading control (**f**). Full length RII-3 (40 kDa) were recognized by all mAbs, whereas N1 (24 kDa), N2 (28 kDa), N3 (30 kDa) and N4 (34 kDa) were selectively recognized by RH1 mAbs. Molecular sizes are indicated on the left (in kDa). Two regions shown in (**a**) (red, from 692 to 726aa and yellow from 746 to 773aa) indicate the targeting regions against mAbs C50 and C2, C41 and C49 respectively. (**g**) Biotinylated peptides (P1-P6) were designed according to the recognition of mAbs to the sequences (green box, from 740 to 795aa) derived from RII-3 (blue box, from 500 to 833aa). The sequences of P1 to P6 were shown. The letters in green were the overlap regions. (**h**) Identification of a linear epitope in PfRH1. C2 and C41 exhibited stronger recognition to peptide P3 than C49. C50 has no interaction with any of the peptides. The cut off value is indicated in red. Any value that is below the cut off value is considered background. The cut off value is calculated by using the formula: (average of Y + 3 x Z), where Y= the lowest 25 percentile of the readings; Z= standard deviation of Y.

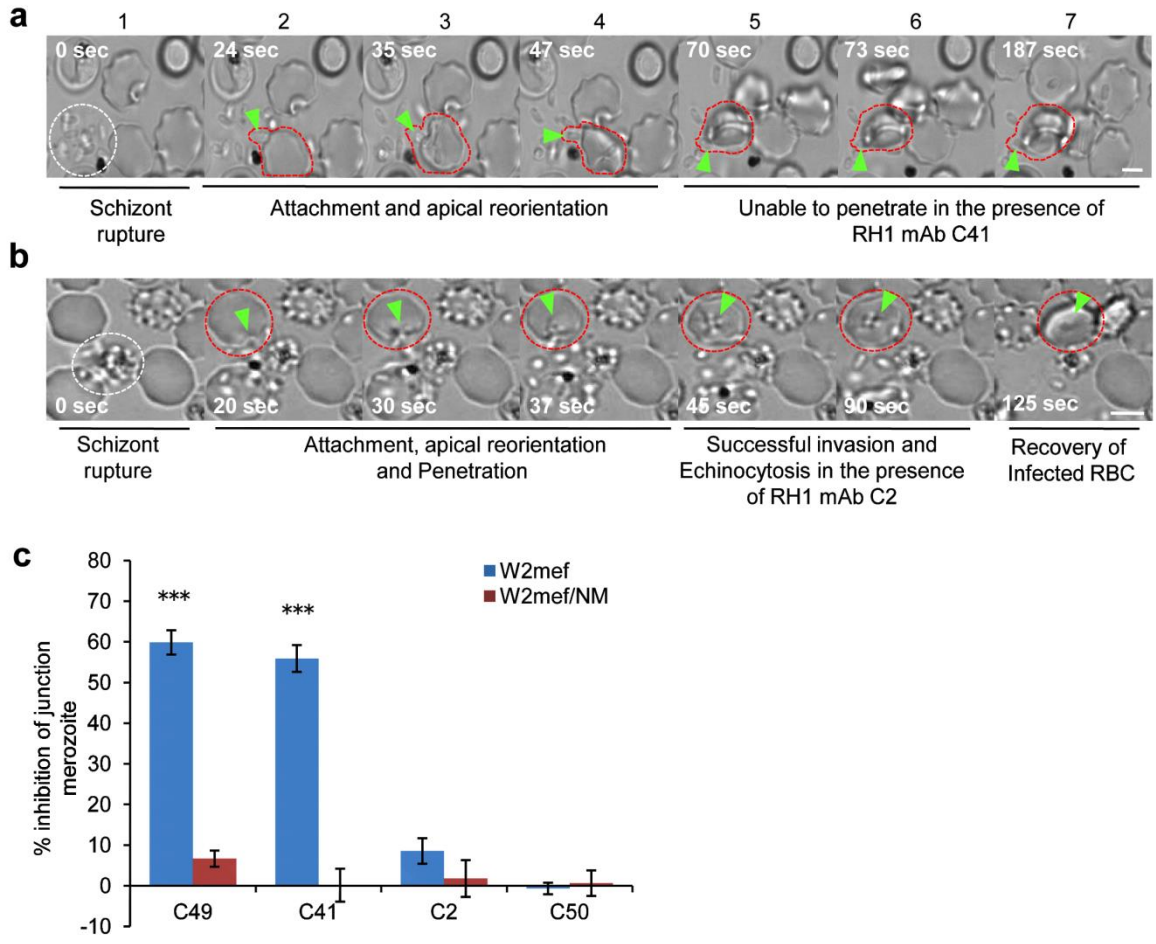

Supplementary Figure S4: Inhibitory mAbs block the invasion before junction formation. (**a-b**) Snapshots were taken from time-lapse live video microscopy of invasion of W2mef merozoite in the presence of inhibitory mAbs C41 and non-inhibitory mAbs C2. Time elapsed post schizont rupture is indicated in each snapshot in seconds (sec, white). White dotted circle indicates rupturing schizont. Green arrow points the merozoites. Red dotted circle follow the infection of erythrocyte by merozoite. Scale bars = 5 µM. (**a**) In the presence of C41 (0.2 mg/ml), the merozoite released from mature schizont (white cycle) (1) attaches and apically reorients (2-4) but unable to penetrate the erythrocyte in spite of the massive force created by the merozoite (5-7) even after 3 min. (**b**) However, the merozoite in the presence of non-inhibitory mAbs C2 (0.2 mg/ml), the merozoite released from mature schizont (white cycle) (1) attaches, apically reorients and penetrates into an uninfected erythrocyte (red circle) (2-4). Following successful invasion deformation of infected erythrocytes occurs (Echinocytosis) (5-6) and by 2 min the erythrocytes recover back to its normal shape (7). Also see Supplementary Movies 3, 4, 5, 6 and 7. (**c**) Inhibitory mAbs significantly reduce the merozoite junction formation in W2mef and W2mef/NM parasites. Schizonts were pretreated with Cyto D and allowed to rupture in the absence or presence of PfRH1 mAbs (0.2 mg/ml). Bar chart indicates the counting of junction-arrested merozoites with mAbs C2, C41, C49 and C50 in W2mef and W2mef/NM compared to the arrested parasites in the absence of mAbs. Inhibitory mAbs C49 and C41 significantly blocked merozoite junction formation in W2mef. Data represents mean±s.e.m., $n = 3$.***$P \leq 0.00003$ by one-way ANOVA, indicating the significant different between the inhibitory mAbs (C49 and C41) and non-inhibitory mAbs (C2 and C50).

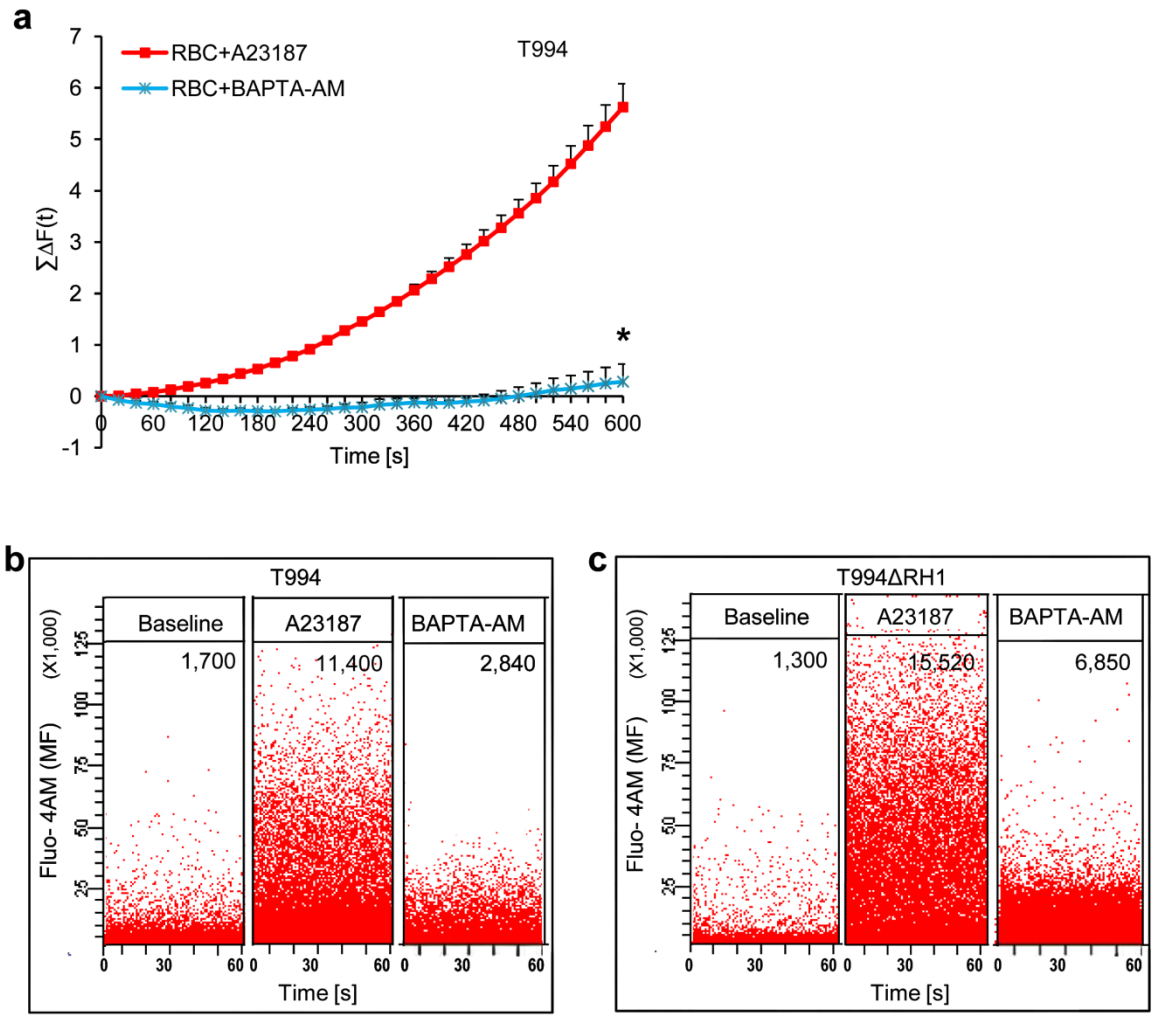

Supplementary Figure S5: Cytosolic Ca^{2+} levels were detected under treatment with Ca^{2+} modulating agents using fluorescence plate reader and Flow Cytometry. (**a**) Preloaded T994 merozoites with Fluo-4AM were incubated with erythrocytes in the presence of Ca^{2+} ionophore A23187 (RBC+A23187) or pre-treatment with Ca^{2+} chelator BAPTA-AM (RBC+BAPTA-AM) respectively. Cytosolic Ca^{2+} levels during merozoite invasion were assessed over time using fluorescence plate reader. The total changes of Ca^{2+} levels ($\sum\Delta F(t)$) in merozoites along the 600 s were summed up and plotted against time (s). Rise in intracellular Ca^{2+} levels by A23187 can be dramatically abolished by Ca^{2+} chelator BAPTA-AM. Cytosolic Ca^{2+} levels were also measured on free merozoites of T994 (**b**) and T994ΔRH1 (**c**) by BD LSR II. Merozoites preloaded with Fluo-4AM were treated with A23187 (A23187) or pretreated with BAPTA-AM followed by A23187 (BAPTA-AM). Preloaded merozoites in completed RPMI only were measured as baselines (Baseline). Data was recorded by using dot plot of Fluo-4 AM mean fluorescence (MF) (list at up-right corners of each sample) *vs* time (s) using BD FACSDiva software to visualize the cytosolic Ca^{2+} levels in merozoites. Every single event is expressed as a separate dot in red indicting its Ca^{2+} level by MF. Data are collected from three biological replicates (Statistical analysis shown in Supplementary Table S2). Experimental data were presented as the mean ± s.e.m.;$n = 3$. *$P \leq 0.0001$ by one-way ANOVA, indicating that BAPTA-AM significantly blocked the A23187 induced Ca^{2+} signaling in T994.

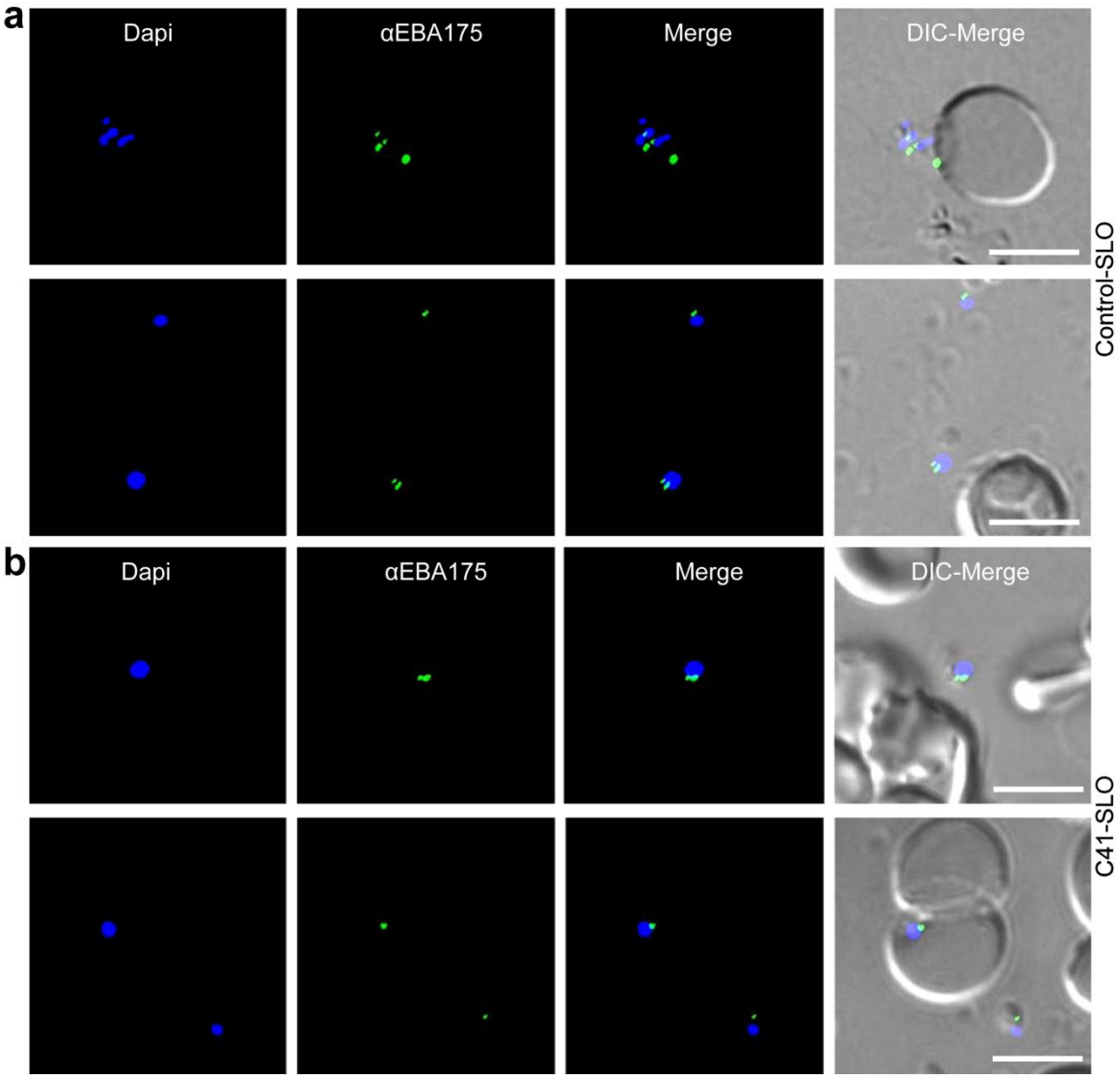

Supplementary Figure S6: EBA175 expression was detected by IFAs in T994 merozoites permeabilized with SLO. IsolatedT994 merozoites were directly incubated with erythrocytes containing 4 µM Cyto D in the absence (**a**) and presence of C41 (0.2 mg/ml) (**b**) followed by incubation with SLO (Control-SLO and C41-SLO) prior to analysis of expression of EBA175. Both DIC and fluorescence images were captured. Nuclear DNA was counterstained with DAPI (blue). EBA175 is shown in green. Fluorescence images, merged fluorescence images (DAPI and green) and merged fluorescence images with DIC images are shown. Scale bars = 10 µM.

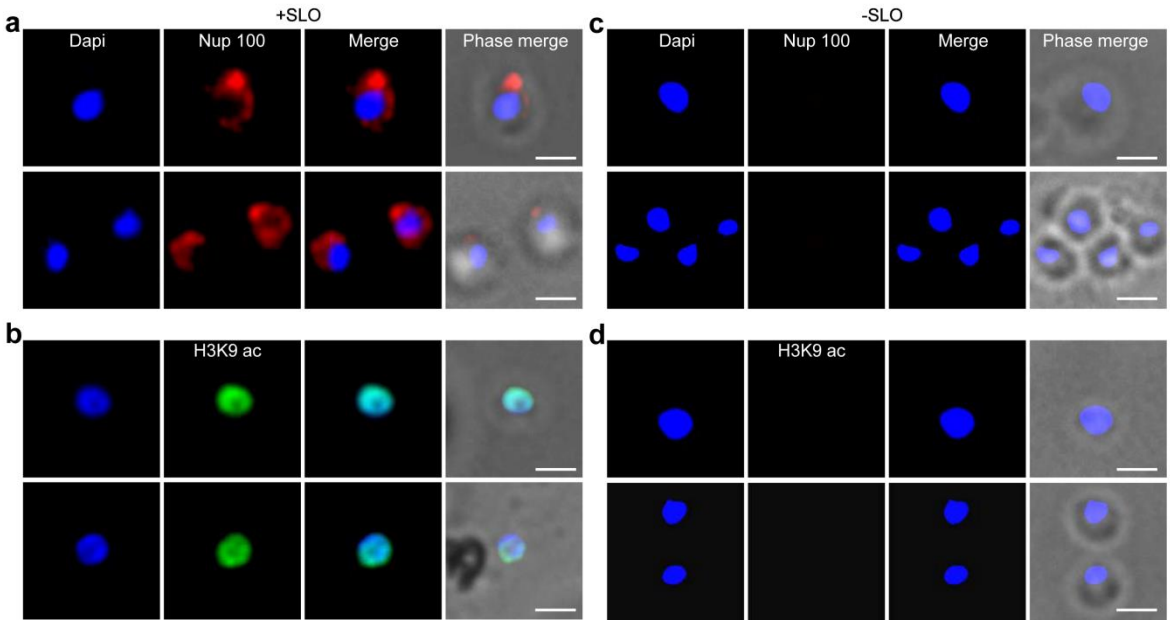

Supplementary Figure S7: Immunofluorescence assay of merozoites permeabilized with SLO. Isolated T994 merozoites were incubated with (**a, b**) or without (**c**, **d**) SLO prior to analysis of Nup 100 (**a, c**) or H3K9ac (**b, d**) respectively. Both phase and fluorescence images were captured. Nuclear DNA was counter stained with DAPI (blue). Nup 100 is shown in red, while H3K9ac in green. Fluorescence images, merged fluorescence images (DAPI and green) and merged fluorescence images with phase images are shown. Scale bars = 10 μM.

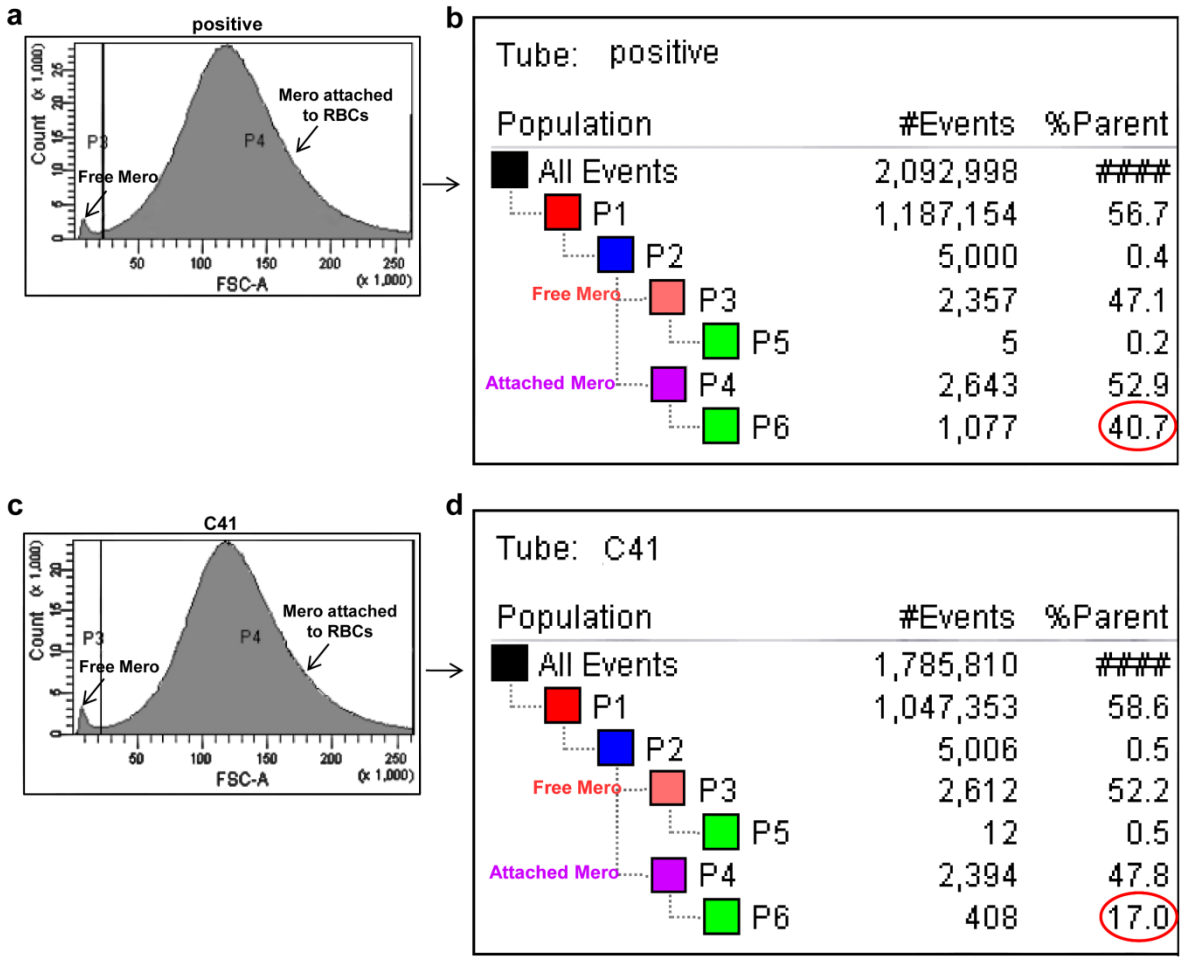

Supplementary Figure S8: Merozoite EBA175 surface expression was analyzed by Flow Cytometry during the invasion. Isolated T994 merozoites were directly incubated with fresh erythrocytes containing 4 µM Cyto D in the absence (**a**, positive) and presence of mAbs C41 (0.2mg/ml) (**c**, C41) as described earlier for the analysis of merozoite surface expression of EBA175 at the tight junction. Data shown here is one representative from four biological replicates. For each experiment about 5,000 DAPI (+) merozoites were captured. Panels (a and c) show the histogram of the two distinct populations observed: un-invaded free merozoites (P3 peak with arrow represents Free Mero) and merozoites bound to uninfected erythrocytes (P4 peak with arrow represents RBC bound merozoites (Mero attached to RBCs)). DAPI (+) cells were gated based on size (FSC-A) for both positive (a) and C41(c), respectively. Panels (**b**) and (**d**) show the gating hierarchy of the populations. The DAPI (+) population P2 (blue) contains both free merozoites (P3, color peach) and attached merozoites (P4, color pink) of which P5 and P6 (green) represents merozoites positive for both DAPI (+) and EBA175 surface expression(+). Data was presented as number of events (#events) and % of parent population (red circle). The value of % Parent population from C41 was compared with that of positive control. The detail of statistical analysis was shown in Figure 6f.

Junction merozoite blocking assay by PfRH1 mAbs												
mAbs (0.2mg/ml)	T994						T994ΔRH1					
	Exp1		Exp2		Exp3		Exp1		Exp2		Exp3	
	No. of junction merozoites	% inhibition	No. of junction merozoites	% inhibition	No. of junction merozoites	% inhibition	No. of junction merozoites	% inhibition	No. of junction merozoites	% inhibition	No. of junction merozoites	% inhibition
Control	103	-	112	-	110	-	290	-	239	-	240	-
C49	44	57.28	42	62.50	41	62.73	279	3.79	233	2.51	246	-2.50
C41	40	61.17	38	66.07	39	64.55	281	3.10	238	0.42	234	2.50
C2	100	2.91	107	4.46	111	-0.91	286	1.38	229	4.18	235	2.08
C50	98	4.85	106	5.36	107	2.73	282	2.76	236	1.26	236	1.67

Supplementary Table S1: Inhibition of junction formation in T994 and T994ΔRH1 by PfRH1 mAbs. T994 or T994ΔRH1 schizonts were pretreated with Cyto D and allowed to rupture in the absence and presence of PfRH1 mAbs (0.2 mg/ml). Junction arrested merozoites were counted microscopically. Table indicates the counting of junction arrested merozoites of 1,000 cells in the absence (Control) or presence of C49, C41, C2 and C50 respectively in T994 and T994ΔRH1. The inhibition effect of mAbs was compared to the controls. Experimental data are presented as the mean ± s.e.m.; $n = 3$.

Inhibition of BAPTA-AM on Ca^{2+} signaling in free merozoites (Mean ± s.e.m.), *n = 3*					
Parasite strain		Fluo-4 AM (MF)		% Inhibition	Mean ± s.e.m.
		A23187	BAPTA-AM		
T994	Exp1	7300	2610	64.25	72.16 ± 3.99
	Exp2	11400	2840	75.09	
	Exp3	10500	2400	77.14	
T994ΔRH1	Exp1	11052	3700	66.52	61.00 ± 3.08
	Exp2	15520	6850	55.86	
	Exp3	10437	4110	60.62	

Supplementary Table S2: Ca^{2+} chelator BAPTA-AM significantly block intracellular Ca^{2+} signaling on free merozoites. Summary of three different experiments on the inhibitory effect of BAPTA-AM on Ca^{2+}signaling by flow cytometry is shown. Experiment 2 (Exp2) is shown as a representative in Supplementary Figure S5b and c. Data is presented as FITC-mean fluorescence (MF). Ca^{2+} levels in the presence of Ca^{2+} chelator, BAPTA-AM, were compared with that in the presence of A23187. BAPTA-AM significantly blocks Ca^{2+} level about 72 and 61% in T994 and T994ΔRH1 respectively. Experimental data are presented as the mean ± s.e.m.

Parasite strain		(%) parasitaemia, *n* = 3		
		Exp1	Exp2	Exp3
T994	RBC	10.8	7.6	11.4
	RBC+C41 (0.2mg/ml)	2.6	3.0	2.3
	RBC+C2 (0.2mg/ml)	10.3	7.2	10.6
T994ΔRH1	RBC	10.8	5.1	10.3
	RBC+C41 (0.2mg/ml)	10.5	5.3	10.1
	RBC+C2 (0.2mg/ml)	10.5	5.0	10.5

Supplementary Table S3: Invasion abilities of isolated merozoites. Merozoites isolated for each of Ca^{2+} measurement experiment were in parallel tested for their invasion capacity. The isolated T994 or T994ΔRH1 merozoites were added to erythrocytes in the absence (control) or presence of mAbs (C41 or C2) at 0.2 mg/ml. The blood smears were made after 24-30 h post-invasion. A total of 1,000 to 2,000 cells were counted. (%) parasitemia = number of ring-infected erythrocytes/total number of cells × 100. Data was presented from three biological replicates.

EBA175 surface expression on merozoite during invasion, n = 3									
T994		EBA175				MSP1			
		F_{EBA175}	$F_{EBA175\text{-}Dapi}$	ratio of $F_{EBA175}/F_{EBA175\text{-}Dapi}$	% inhibition of EBA175 surface expression	F_{MSP1}	$F_{MSP1\text{-}Dapi}$	ratio of $F_{EBA175}/F_{EBA175\text{-}Dapi}$	% inhibition of MSP1 surface expression
Exp1	Control	16749	38246	0.4379	39.6302	33967	29078	1.1681	0.6314
	C41	11512	43544	0.2644		41583	35824	1.1608	
Exp2	Control	31683	31201	1.0154	32.1389	41707	41119	1.0143	0.1954
	C41	26065	37825	0.6891		40844	40347	1.0123	
Exp3	Control	32919	30656	1.0738	39.8190	40630	40451	1.0044	0.3551
	C41	24102	37296	0.6462		40804	40769	1.0009	
T994ΔRH1		EBA175				MSP1			
		F_{EBA175}	$F_{EBA175\text{-}Dapi}$	ratio of $F_{EBA175}/F_{EBA175\text{-}Dapi}$	% inhibition of EBA175 surface expression	F_{MSP1}	$F_{MSP1\text{-}Dapi}$	ratio of $F_{EBA175}/F_{EBA175\text{-}Dapi}$	% inhibition of MSP1 surface expression
Exp1	Control	18669	43314	0.4310	2.6115	41559	38417	1.0818	3.4210
	C41	15801	37643	0.4198		39898	38188	1.0448	
Exp2	Control	23740	28802	0.8242	0.3160	42689	27596	1.5469	2.1836
	C41	25397	30910	0.8216		44880	29660	1.5131	
Exp3	Control	29768	32413	0.9184	0.6630	43474	42512	1.0226	2.0586
	C41	28433	31166	0.9123		42548	42481	1.0016	

Supplementary Table S4: EBA175 surface expression on merozoite during invasion was detected by fluorescence plate reader. Fluorescence signal of EBA175 (F_{EBA175}), MSP1 (F_{MSP1}) and nuclei ($F_{EBA175\text{-}Dapi}$ and $F_{MSP1\text{-}Dapi}$) of T994 and T994ΔRH1 were excited and emitted at the appropriate wavelength. Fluorescence signal measurement is presented from three biological replicates. Surface expression of EBA175 and MSP1 on merozoite in the presence of C41 (C41) was compared to their controls (Control). The effect of C41 was presented as % inhibition of EBA175 surface expression. Experimental data are presented as the mean ± s.e.m.; *n* = 3.

EBA175 expression on T994 merozoitepermeabilizedwith SLO, *n = 3*						
		F_{EBA175}	$F_{EBA175\text{-}Dapi}$	ratio of $F_{EBA175}/F_{EBA175\text{-}Dapi}$	% inhibition of EBA175 expression	Mean ± s.e.m.
Exp1	Control-SLO	41233	35601	1.1582	1.9839	0.89 ± 0.59
	C41-SLO	39307	34625	1.1352		
Exp2	Control-SLO	45096	39687	1.1363	0.7280	
	C41-SLO	34840	30886	1.1280		
Exp3	Control-SLO	29479	22587	1.3051	-0.0469	
	C41-SLO	26850	20563	1.3057		

Supplementary Table S5: EBA175 expression on T994 merozoite permeabilized with SLO during invasion. Isolated T994 merozoites were directly incubated with erythrocytes containing 4 μM Cyto D in the absence or presence of C41 (0.2 mg/ml) followed by treatment with SLO. EBA175 expression on merozoite was detected by fluorescence plate reader. Fluorescence signal of EBA175 and nuclei were excited and emitted at the appropriate wavelength. Expression of EBA175 on merozoite in the presence of C41 (C41-SLO) was compared to their controls (Control-SLO). Experimental data are presented as the mean ± s.e.m.; $n = 3$.